Applied Surface Science 321 (2014) 103–108

Contents lists available at ScienceDirect

Applied Surface Science

journal homepage: www.elsevier.com/locate/apsusc

Surface modification and characterization of aramid fibers with hybrid coating

Jianrui Chen, Yaofeng Zhu, Qingqing Ni, Yaqin Fu*, Xiang Fu

The Key Laboratory of Advanced Textile Materials and Manufacturing Technology Ministry of Education, Zhejiang Sci-Tech University, Hangzhou Zhejiang 310018, China

ARTICLE INFO

Article history:
Received 17 July 2014
Received in revised form
29 September 2014
Accepted 29 September 2014
Available online 7 October 2014

Keywords:
Aramid fiber
Hybrid coating
Surface modification
Interfacial adhesion

ABSTRACT

Aramid fibers were modified through solution dip-coating and interfacial in situ polymerization using a newly synthesized SiO_2/shape memory polyurethane (SiO_2/SMPU) hybrid. Fourier transform infrared and X-ray photoelectron spectroscopy indicated that the synthesized SiO_2/SMPU hybrid successfully coated the fiber surface. The surface morphology of the aramid fibers and the single fiber tensile strength and interfacial shear strength (IFSS) of the composites were determined. The IFSS of the fiber coated with the hybrid improved by 45%, which benefited from a special "pizza-like" structure on the fiber surface.

1. Introduction

Fiber-reinforced polymer composites are widely used in aerospace, automotives, and industries because of their outstanding properties, such as high specific strength, low density, and flexible design [1,2]. Composite interfaces must efficiently transfer stress from the matrix to the fibers to optimize the mechanical performance of fiber-reinforced polymer composites [3,4]. Therefore, the fiber–matrix interface has been a research hotspot.

Aramid fibers are high-performance fibers that have attracted commercial and academic interest because their highly crystalline structure offers high specific toughness ratio and strength [5,6]. However, aramid fiber-reinforced polymer composites demonstrate poor interfacial adhesion because aramid fibers exhibit chemical resistance to the active groups of the polymer matrix [7,8].

Many prominent researchers investigated different methods to improve the interface of aramid fiber-reinforced polymer composites. One of these methods is modifying the aramid fiber surface through chemical or physical treatments, such as coupling agent and surface grafting, plasma treatment, γ-rays, and ultrasound [9–13], or modifying the original resin matrix to match the aramid fiber [14,15].

Coating is an important fiber surface modification method that has shown promising interface improvement. This method has the advantages of retaining the main fiber structure, fixing defects on the fiber surface, and being suitable for complex-shaped samples [16–18]. Many coating treatments have been used to modify the aramid fiber surface, but limited success has been achieved. Lange et al. [19] found that polyurethane varnish coating can significantly improve the interfacial properties of aramid/epoxy resin composites. Zou et al. [20] reported that nano-SiO_2 coating using the sol–gel method can improve the mechanical properties of aramid filaments. However, studies have rarely analyzed the potential use of inorganic nanofiller/polyurethane hybrid materials in fiber coating.

Aramid fibers were modified in the present work by solution dip-coating and interfacial in situ polymerization using a newly synthesized SiO_2/shape memory polyurethane (SiO_2/SMPU) hybrid. The microstructure of the SiO_2/SMPU hybrid was investigated. The aramid fiber surface topography and SiO_2 nanoparticle distribution of the hybrid coating the aramid fiber were determined through scanning electron microscopy. The tensile properties of the coated aramid fibers were tested in the fiber direction using universal testing instruments. The adhesion between the modified aramid fibers and the resin matrix was also evaluated through interfacial shear strength (IFSS) to analyze the fiber–matrix interface properties.

2. Experimental

Aramid fibers (Twaron2200, with 13 μm diameter) were supplied by Teijin Japan and liquid shape memory polyurethane (Diary, MS-4510) was supplied by Diaplex Co. Ltd. Japan.

* Corresponding author. Tel.: +86 571 86843607; fax: +86 571 86843607.
E-mail address: fyq01@zstu.edu.cn (Y. Fu).

http://dx.doi.org/10.1016/j.apsusc.2014.09.196
0169-4332/

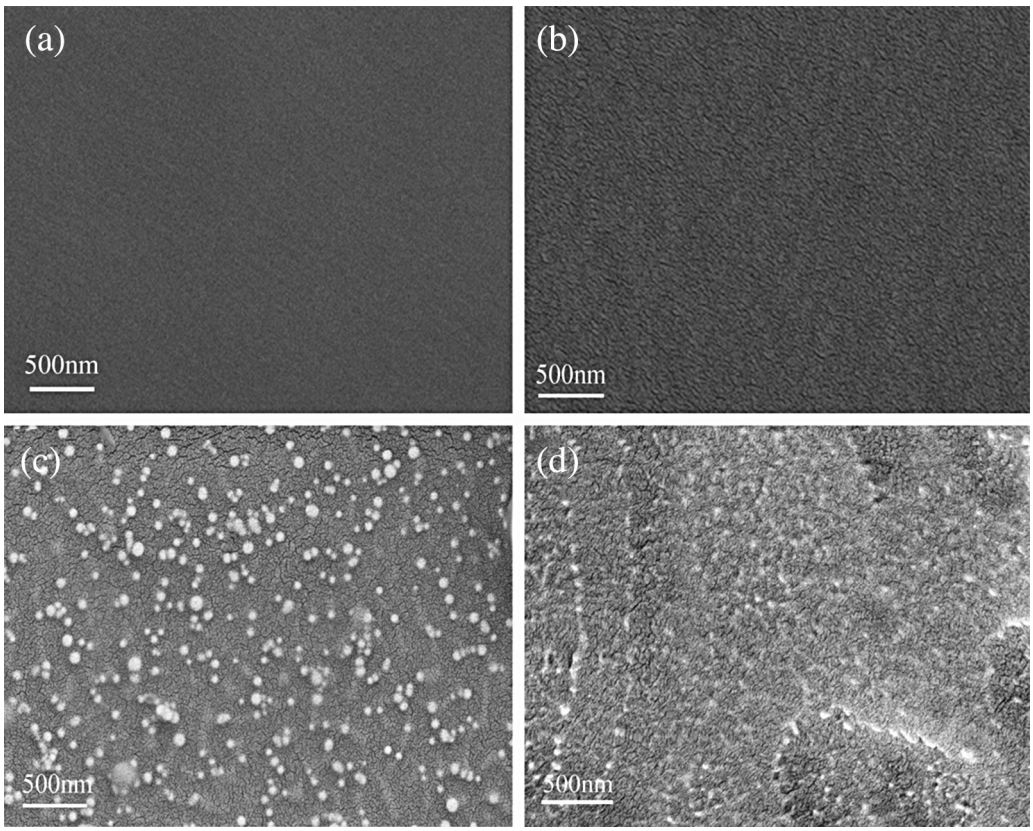

Fig. 1. SEM images of pure SMPU (a) surface and (b) cross-section, and SiO_2/SMPU (c) surface and (d) cross-section.

Tetraethoxysilane (TEOS), 3-aminopropyltriethoxysilane (KH550), p-toluenesulfonic acid (PTSA), N,N-dimethylacetamide (DMAc), phosphoric acid, acetone, and absolute ethanol were of analytical grade.

2.1. SMPU/SiO_2 hybrid synthesis

The SiO_2 precursor (solution A) was prepared by mixing PTSA, TEOS, and DMAc at a mass ratio of 0.1:10:100 under stirring at 25 °C for 2 h. The modified SMPU resin (solution B) was prepared by mixing SMPU resin and KH550 at a mass ratio of 100:2 under stirring at 50 °C for 2 h. The SiO_2/SMPU hybrid was synthesized by mixing solutions A and B under stirring at 50 °C for 2 h. The equivalent PTSA/TEOS/KH550 was ensured to be 0.1:10:2. The final hybrid used to coat the aramid fibers was prepared by mixing the SiO_2/SMPU hybrid and DMAc at a mass ratio of 2:100.

2.2. Surface modification of aramid fibers

The aramid fibers were washed in acetone and subjected to functionalized pretreatment using 30% aqueous phosphoric acid solution at 40 °C for 2 h. The sample was dried and marked as TF. TF was coated with pure SMPU and SiO_2/SMPU through the dipping method and then dried at room temperature for 2 days. The samples were designated as SMPU–TF and S–TF, respectively.

2.3. Preparation of single fiber-reinforced composite

SMPU was poured into molds fixed with single aramid fibers. The molds were heated in an oven to 40 °C for 24 h, 60 °C for 24 h, 80 °C for 24 h, and 24 h at 130 °C.

2.4. Characterization

The morphology of the SiO_2/SMPU materials and S–TF were examined through field-emission scanning electron microscopy (F-ESEM) (ULTRA 55, ZEISS, Germany). Attenuated-total-reflection infrared spectra were recorded using a Nicolet5700 FT-IR spectrometer (Thermo Electron, USA) to analyze the chemical structures of the aramid fibers. X-ray photoelectron spectroscopy (XPS) was performed using an ESCALAB MARK II X-ray photoelectron spectrometer (VG, U.K.).

The tensile strength of the coated fibers was determined using a universal testing instrument (KES-G1, Japan) at a rate of 6.0 mm/min in accordance with GJB993-1990. Single-fiber fragmentation testing was performed by a Leica DM2700P polarizing microscope. The IFSS was calculated according to the saturated number of cracks throughout the fiber using the equation:

$$IFSS = k\frac{\sigma_f d}{2\bar{l}},$$

where k is the correction factor for aramid fiber (k = 0.889) [21], σ_f is the ultimate fiber strength at the critical length, d is the fiber diameter, and $\bar{l}$ is the average fiber fragment length.

3. Results and discussion

3.1. Characterization and analysis of SiO_2/SMPU hybrid structure

Typical SEM images of SMPU and SiO_2/SMPU hybrid are shown in Fig. 1. SiO_2 particles with sizes ranging from 30 to 50 nm are evenly distributed both on the surface (Fig. 1c) and on the cross-section (Fig. 1d) compared with the smooth SMPU (Fig. 1a and 1b). This result can be attributed to the fact that the hydrolysis

condensation of the system is well controlled through the anhydrous sol–gel method, which uses water in air as the hydrolysis reaction source [15]. Meanwhile, SMPU and TEOS interact through the amino and alkoxy groups of KH550, respectively. This interaction not only forms covalent bonds between the organic polymer and inorganic silica but also prevents particle agglomeration. Therefore, the nanoparticles exhibit excellent dispersion and suitable size, and the sizing system shows stability even after six months.

3.2. Structure and properties of the aramid fiber surface

The FTIR spectra of the TF and S–TF samples are shown in Fig. 2. The characteristic bands of TF at 3320 and 1543 cm^{-1} are attributed to the N–H vibration of the primary amine in Twaron. Absorption peaks at 2958, 1729, 1610, and 1222 cm^{-1} are absent in TF but present in S–TF. This result can be ascribed to the characteristic peaks of polyurethane. The sharp absorption peak at 1067 cm^{-1} can also be ascribed to the characteristic peaks of Si–O–Si, which are created because of the formation of sizing through the hydrolysis and condensation of the precursor (SMPU + KH550 + TEOS). The absorption peaks are relatively weak because of the relatively low amount of hybrid coated on the fibers.

The chemical microstructure of S–TF as determined through XPS is shown in Fig. 3. The wide-scan spectra of the TF (Fig. 3a) and S–TF (Fig. 3c) surfaces contain C 1s, N 1s, and O 1s peaks. The N 1s peak intensity of S–TF is lower than that of TF. This result indicates that the coating on the S–TF surface has a lower nitrogen ratio than that on the TF surface. Fig. 3b shows that the N 1s core-level spectrum of the TF surface contains only two peaks. These peaks can be ascribed to the N–H and N–C species at binding energies (BEs) of 399.5 and 399.1 eV, respectively, caused by TF synthesis. The N 1s core-level spectrum of S–TF (Fig. 1d) can be curve-fitted with three peak components, with a new one for the N–Si species at a BE of 397.8 eV.

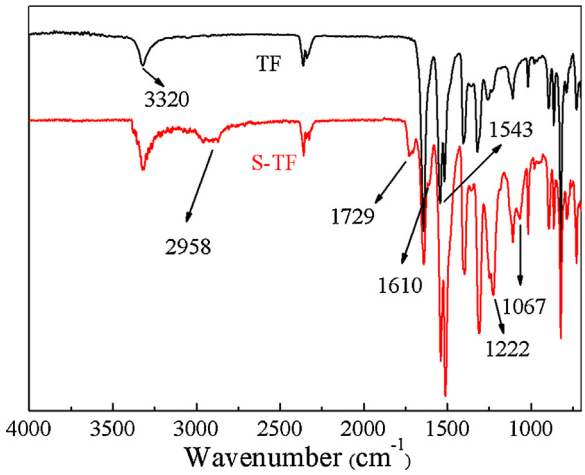

Fig. 2. FTIR spectra of TF and S–TF fibers.

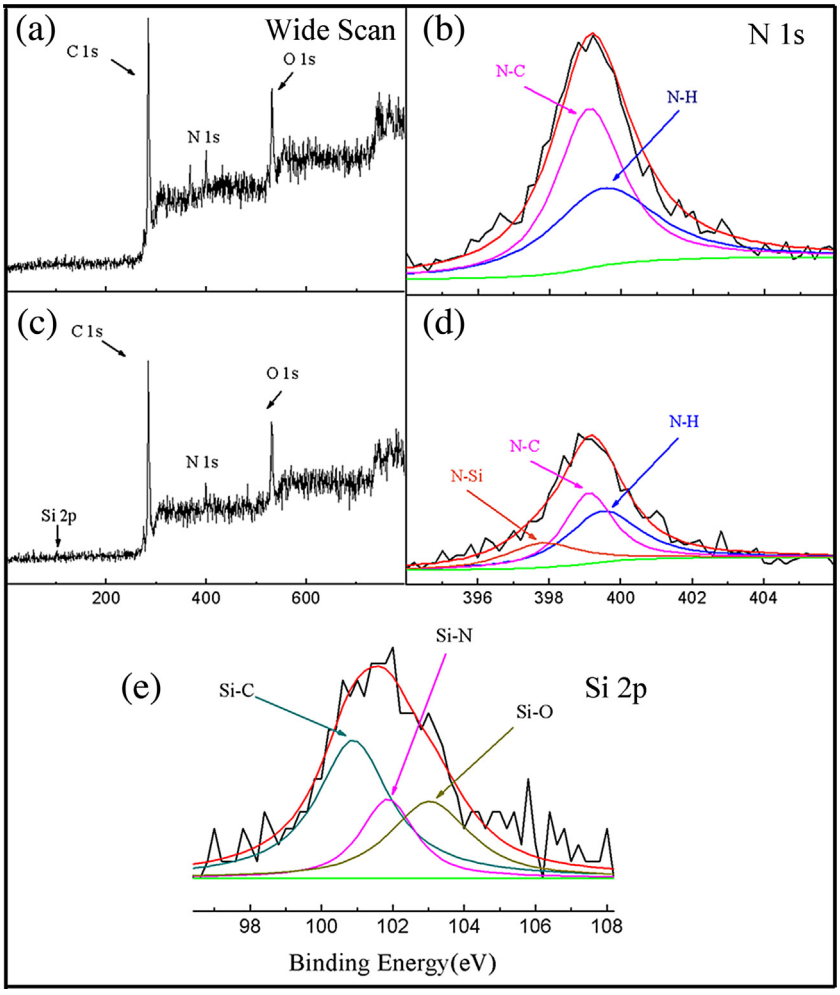

Fig. 3. XPS spectra of (a and b) TF and (c, d and e) S–TF fibers.

Table 1
Elemental composition of the sample surfaces.

Sample	Atomic percent				Atomic ratio
	C 1s	O 1s	N 1s	Si 2p	O/N
TF	76. 84	15. 44	7. 72	0	2. 00
S–TF	76. 32	16. 32	5. 02	2. 34	3. 25

The Si 2p core-level spectrum of S–TF (Fig. 3e) can be curve-fitted with three peak components, namely, 28.9% Si–O, 51.1% Si–C, and 20.0% Si–N. This result suggests that silicon exists in the forms of SiO_2 and covalent cross-linking oxide.

The surface elemental composition of the samples is listed in Table 1. The O/C ratio is increased and the oxygen element is increased by 6% after the modification. The nitrogen element ratios of TF and S–TF are 7.72 and 5.02, respectively, and the O/N ratios of TF and S–TF are 2.00 and 3.25, respectively. The increase in O/N on the polar surface probably contributes to the adhesion between the fiber and the matrix [22]. The S–TF surface contains 2.34% Si. FTIR and XPS analyses indicate the successful coating of the SiO_2/SMPU hybrid onto the aramid fiber surface.

Fig. 4 shows the surface morphology of the aramid fibers. Slight lines and grooves as well as plush-like microfibers can be observed on the TF surface (Fig. 4a). The SMPU–TF surface contains a coarse SMPU membrane (Fig. 4b). However, the S–TF surface contains an integrated compact membrane with embedded and semi-embedded particles (Fig. 4c and 4d). The great number of particles uniformly scattered on the fiber surface plays an important role in increasing the specific surface area.

Single-fiber tensile testing was performed to characterize in-plane strength (Fig. 5). Coating increases fiber strength; S–TF is stronger than SMPU–TF. This result and mechanism can be explored as follow: a special structure was introduced onto the S–TF surface with some reactive groups after acidification. Reactive groups react with silicon hydroxyl groups and form Si–O–Si bonds during drying. As a result, a silicon-oxide network structure is constructed. This structure improves network structure uniformity, enhances stress transfer, and then improves fiber anti-load capacity and tensile strength. This phenomenon can be referred to as the "surround effect" of hybrid membrane. SEM and XPS spectral analyses show that the SMPU/SiO_2 hybrid on the aramid fiber surface has a "pizza-like" structure (Fig. 6). SiO_2 particles are located outside and covalent cross-linking oxide membranes are located inside this structure. The formation of this structure is a major advantage because previous fiber surface modification efforts to increase

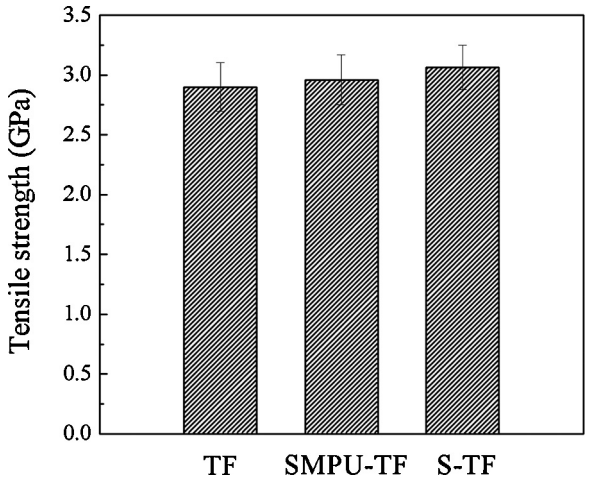

Fig. 5. Tensile strength of monofilament aramid fibers modified through different methods.

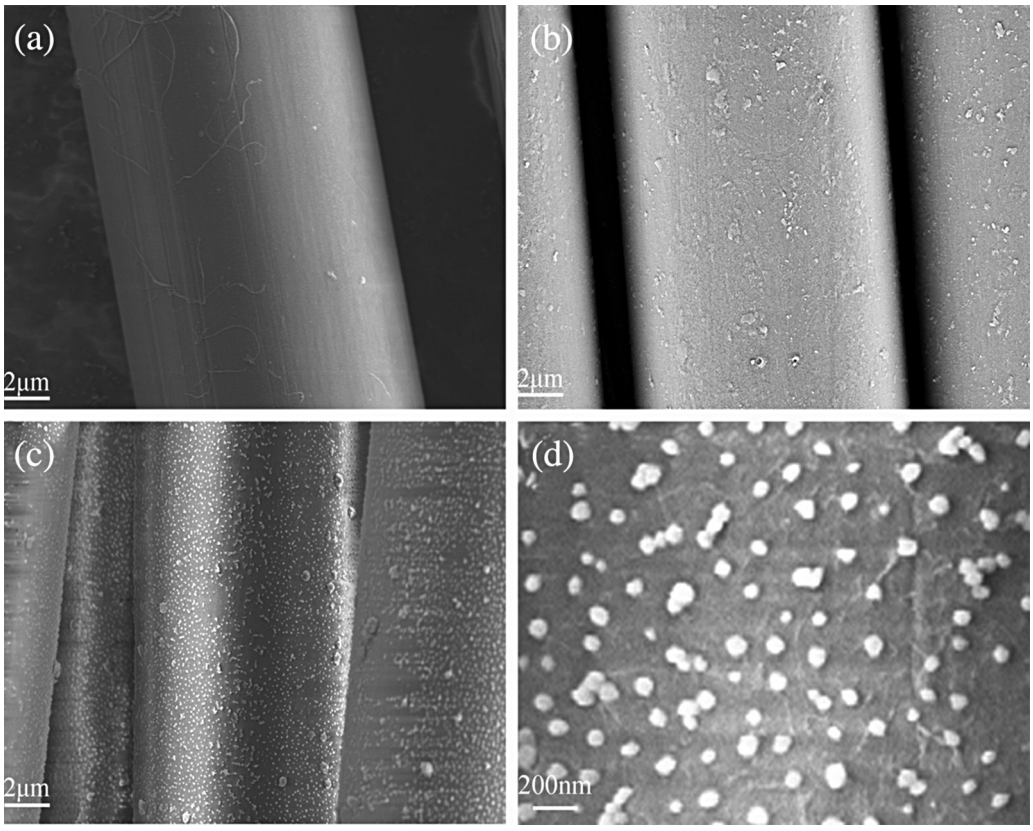

Fig. 4. SEM images of the aramid fibers surface (a: TF; b: SMPU–TF; c and d: S–TF).

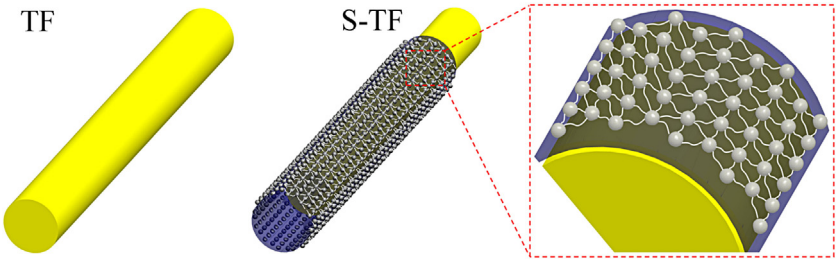

Fig. 6. Schematic of aramid fiber modified with SiO_2/SMPU hybrid.

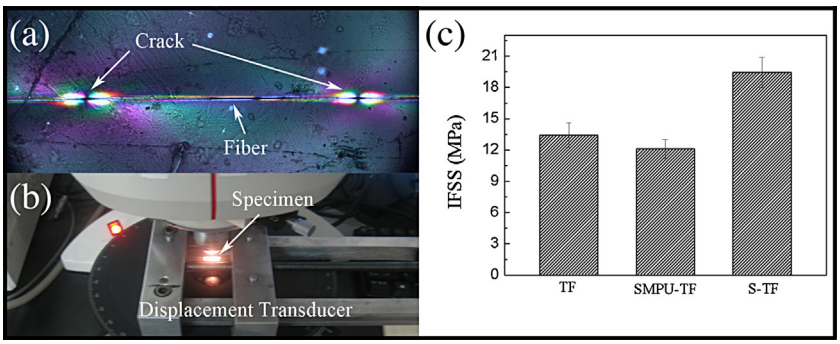

Fig. 7. Single-fiber segmentation results. (a) Micrograph of the typical fiber cracks, as observed in situ during the test. (b) Microtensile frame used in the testing, with a specimen in its jaws. (c) showing a 45% increase in single-fiber interfacial strength. The three fibers tested were TF, SMPU–TF, and S–TF.

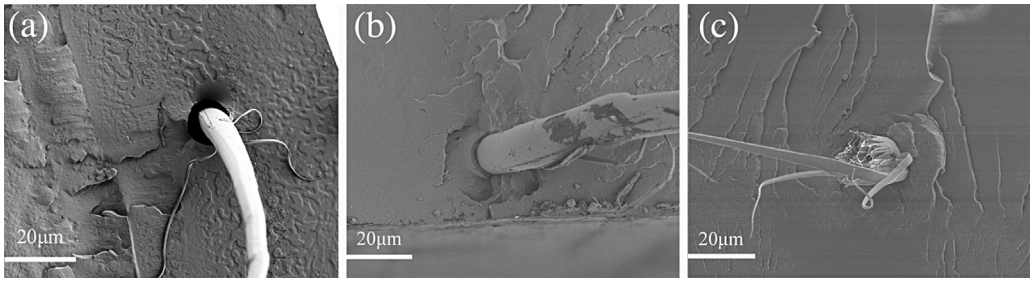

Fig. 8. Brittle cross-section morphology of the aramid fiber/SMPU composites: (a) TF fiber/SMPU, (b) SMPU–TF fiber/SMPU, and (c) S–TF fiber/SMPU.

adhesion with the matrix improve interfacial properties but at the cost of fiber strength.

3.3. Evaluation of interfacial adhesion

The interfacial properties of the fiber after surface treatment were evaluated through single fiber fragmentation. This process is widely used to assess interfacial strength [23]. The samples were placed in a screw-driven microtensile test stage, stress was applied on the specimen, and the specimen was monitored using an optical microscope under polarized light (Fig. 7a). The number of fragments was counted under increasing strain using this system to identify the saturation point (Fig. 7b). The number of fragments was then used to determine critical length. The interfacial shear strength of each case studied is plotted in Fig. 7c. The interfacial strength of S–TF is 45% higher than that of TF. The interfacial adhesion between the aramid fiber and the polymer matrix is significantly increased after the modification. However, the counter interfacial strength of SMPU–TF is decreased. Therefore, the new structure of the S–TF surface indicates strong adhesion between the fiber and the matrix.

The cross-sections of the specimens under SEM are illustrated in Fig. 8. Fig. 8a shows that the TF forms plastic flow necking near the fracture in the longer range. This finding may be attributed to the acidification pretreatment [24]. However, the SMPU membrane detaches from the SMPU–TF surface, and the fiber surface shows irregular mottles (Fig. 8b). This result may be attributed to the different thermal expansion coefficients of the pure SMPU coating and aramid fibers [25]. However, axial splitting and many fibrillated and petaloid microfibers are found in S–TF (Fig. 8c). This result suggests that S–TF exhibits more consumed fracture energies and better interfacial bonding than TF. The excellent interfacial adhesion is expected to exert the “hammer ball effect” on the particles from the “pizza-like” structure coating. The links point between the matrix and the fiber, showing that the “pizza” combines with the two interfaces by covalently linking the cross-linking oxide membrane to the fiber and linking the SiO_2 particles to the matrix. The “hammer ball” is pulled when the reinforced fibers are forced, and the stress is efficiently transferred from the matrix to the fibers. The SEM micrographs of the fracture surface of the species correspond well to the IFSS testing results.

4. Conclusions

A novel SiO_2/SMPU hybrid was synthesized by the anhydrous sol–gel method, and nanoparticles of excellent dispersion and suitable size were successfully obtained. The aramid fibers were modified using the synthesized hybrid. FTIR, XPS, and SEM indicated that the hybrid was formed on the aramid fiber surface

after modification. Hybrid modification increased single fiber tensile strength by 5.7% and improved the IFSS of the S–KF composite by 45%. A "pizza-like" structure was also formed in the hybrid on the fiber surface during coating. The interfacial phase structure possessed both inorganic composition and organic structure. This special phase structure can improve performance, particularly at the interfacial bonding area. Hybrid modification effectively and conveniently improved the interface properties between the fibers and the matrix as well as the mechanical properties of aramid fibers. This method is expected to be an important direction for future research on aramid fiber surface modification.

Acknowledgments

The authors gratefully acknowledge the Instrumental Analysis Center of Zhejiang Sci-Tech University for the use of their characterization facilities. We also thank the technicians for their assistance in the analyses and for the technical discussions.

References

[1] C.E. Bakis, L.C. Bank, V.L. Brown, E. Cosenza, J.F. Davalos, J.J. Lesko, A. Machida, S.H. Rizkalla, T.C. Triantafillou, Fiber-reinforced polymer composites for construction-state-of-the-art review, J. Compos. Constr. 6 (2002) 73–87.
[2] F.M. AL-Oqla, S.M. Sapuan, Natural fiber-reinforced polymer composites in industrial applications: feasibility of date palm fibers for sustainable automotive industry, J. Clean. Prod. 66 (2014) 347–354.
[3] F.Z. Arrakhiz, M.E. Achabya, M. Malha, M.O. Bensalah, O. Fassi-Fehri, R. Bouhfid, K. Benmoussa, A. Qaiss, Mechanical and thermal properties of natural fibers reinforced polymer composites: Doum/low density polyethylene, Mater. Des. 43 (2013) 200–205.
[4] S.S. Nair, D.C. Hurley, S. Wang, T.M. Young, Nanoscale characterization of interphase properties in maleated polypropylene-treated natural fiber-reinforced polymer composites, Polym. Eng. Sci. 53 (2013) 888–896.
[5] I.M. Daniel, O. Ishai, Engineering Mechanics of Composite Materials, 2nd ed., Oxford University Press, New York, 2006.
[6] J.M. García, F.C. García, F. Serna, J.L. de la Peña, High-performance aromatic polyamides, Prog. Polym. Sci. 35 (2010) 623–686.
[7] W. Wang, R. Li, M. Tian, L. Liu, H. Zou, X. Zhao, L. Zhang, Surface silverized meta-aramid fibers prepared by bio-inspired poly(dopamine) functionalization, ACS. Appl. Mater. Interfaces 5 (2013) 2062–2069.
[8] G.J. Ehlert, H.A. Sodano, Zinc oxide nanowire interphase for enhanced interfacial strength in lightweight polymer fiber composites, ACS. Appl. Mater. Interfaces 1 (2009) 1827–1833.
[9] T. Ai, R. Wang, W. Zhou, Effect of grafting alkoxysilane on the surface properties of Kevlar fiber, Polym. Compos. 28 (2007) 412–416.
[10] T.M. Liu, Y.S. Zheng, J. Hu, Surface modification of aramid fibers with new chemical method for improving interfacial bonding strength with epoxy resin, J. Appl. Polym. Sci. 118 (2010) 2541–2552.
[11] M. Su, A. Gu, G. Liang, L. Yuan, The effect of oxygen-plasma treatment on Kevlar fibers and the properties of Kevlar fibers/bismaleimide composites, Appl. Surf. Sci. 257 (2011) 3158–3167.
[12] Y.H. Zhang, Y.D. Huang, L. Liu, K.L. Cai, Effects of γ-ray radiation grafting on aramid fibers and its composites, Appl. Surf. Sci. 254 (2008) 3153–3161.
[13] L. Liu, Y.D. Huang, Z.Q. Zhang, Z.X. Jiang, L.N. Wu, Ultrasonic treatment of aramid fiber surface and its effect on the interface of aramid/epoxy composites, Appl. Surf. Sci. 254 (2008) 2594–2599.
[14] T.K. Lin, S.J. Wu, J.G. Lai, S.S. Shyu, The effect of chemical treatment on reinforcement/matrix interaction in Kevlar-fiber/bismaleimide composites, Compos. Sci. Technol. 60 (2000) 1873–1878.
[15] L. Xu, Y. Fu, M. Du, Investigation on structures and properties of shape memory polyurethane/silica nanocomposites, Chin. J. Chem. 29 (2011) 703–710.
[16] B. Wei, H.L. Cao, S.H. Song, Surface modification and characterization of basalt fibers with hybrid sizings, Compos. Part A. 42 (2011) 22–29.
[17] B. Mahltig, H. Haufe, H. Böttcher, Functionalization of textiles by inorganic sol–gel coatings, J. Mater. Chem. 15 (2005) 4385–4398.
[18] B.S. Shim, W. Chen, C. Doty, C. Xu, N.A. Kotov, Smart electronic yarns and wearable fabrics for human biomonitoring made by carbon nanotube coating with polyelectrolytes, Nano Lett. 8 (2008) 4151–4157.
[19] P.J. de Lange, E. Mäder, K. Mai, R.J. Young, I. Ahmad, Characterization and micromechanical testing of the interphase of aramid-reinforced epoxy composites, Compos. Part A. 32 (2001) 331–342.
[20] J. Zou, Y.C. Zhang, H.Y. Wu, Y.P. Qiu, Nano effects of helium plasma treatment nano-SiO_2 coating Kevlar filaments, Mater. Sci. Forum 610 (2009) 692–699.
[21] P.J. Herrera-Franco, L.T. Drzal, Comparison of methods for the measurement of fiber/matrix adhension in composites, Composites 23 (1992) 2–27.
[22] P.J. de Lange, P.G. Akker, E. Mäder, S.L. Gao, W. Prasithphol, R.J. Young, Controlled interfacial adhesion of Twaron® aramid fibers in composites by the finish formulation, Compos. Sci. Technol. 67 (2007) 2027–2035.
[23] B.W. Kim, J.A. Nairn, Observations of fiber fracture and interfacial debonding phenomena using the fragmentation test in single fiber composites, J. Compos. Mater. 36 (2002) 1825–1858.
[24] G. Li, C. Zhang, Y. Wang, P. Li, Y. Yu, X. Jia, H. Liu, X. Yang, Z. Xue, S. Ryu, Interface correlation and toughness matching of phosphoric acid functionalized Kevlar fiber and epoxy matrix for filament winding composites, Compos. Sci. Technol. 68 (2008) 3208–3214.
[25] L.B. Xu, Y.Q. Fu, Q.Q. Ni, Interfacial properties of aramid/SMPU-SiO_2 composites, Acta Polym. Sin. 10 (2011) 1132–1137.